Korean J. Chem. Eng., **29**(9), 1178-1186 (2012)
DOI: 10.1007/s11814-012-0014-3

Electrochemical degradation of phenol on the La and Ru doped Ti/SnO_2-Sb electrodes

Haiqing Xu*,, Ai-Ping Li**, Qi Qi*,***, Wei Jiang*, and Yue-Ming Sun*,†**

*School of Chemistry & Chemical Engineering, Southeast University, Nanjing 211189, China
**Key Laboratory for Attapulgite Science and Applied Technology of Jiangsu Province, Huaiyin Institute of Technology, Huaian 223003, China
***State Key Lab of Silicon Materials, Zhejiang University, Hangzhou 310027, China
(*Received 29 June 2011 • accepted 8 February 2012*)

Abstract–La and Ru doped Ti/SnO_2-Sb electrodes were prepared by thermal decomposition and characterized by scanning electron microscopy (SEM), X-ray diffraction (XRD) and X-ray photoelectron spectroscopy (XPS). It confirmed that the surface of the La and Ru doped Ti/SnO_2-Sb electrodes presents a certain microspherical structure formed by aggregates of nanoparticles, which increases the specific area greatly and provides more active sites. The enhanced performance of the La and Ru doped electrodes arose from the increased adsorption capacity of hydroxyl radicals. Cyclic voltammetry (CV) and electrochemical impedance spectroscopy (EIS) showed an improvement of the electrochemical capacity for the La and Ru doped Ti/SnO_2-Sb electrodes. The electrochemical oxidation performance of the prepared electrode was further studied using phenol as a model pollutant. UV scans revealed that both phenol and its intermediate products are more rapidly decomposed, especially in the early stage of oxidation on the La and Ru doped electrodes. The removals of chemical oxygen demand (COD) were 86.4% and 82.1% on the Ti/SnO_2-Sb-La and Ti/SnO_2-Sb-Ru electrodes, respectively, which were higher than that on the SnO_2-Sb/Ti electrode (60.1%). The doped electrodes are demonstrated to have superior electrochemical oxidation ability for phenol.

Key words: Electrochemical Oxidation, Ti/SnO_2-Sb-La, Ti/SnO_2-Sb-Ru, Phenol Degradation

INTRODUCTION

Much industrial wastewater containing refractory organic pollutants, such as aromatic hydrocarbons, phenolic compounds and pesticides, due to its toxicity and difficulty to be degraded, becomes an intractable environmental problem and potential hazard towards human and animal health [1]. Conventional biochemical processes fail to treat those organic contaminants. Numerous technologies have been used in treatment process of industrial wastewater, such as chemical oxidation, wet oxidation, photochemical degradation, etc [2-7]. Recently, electrochemical oxidation has become an alternative due to its strong oxidation performance, non-selective oxidation and environmental compatibility [8-10]. Organic pollutants can be destroyed electrochemically by a direct anodic oxidation or an indirect oxidation and effectively degraded to CO_2 or aliphatic products. The treated effluent will become much less toxic and more biodegradable, and so electrochemical degradation can be also used as a pre-treatment technology in detoxifying ahead of bio-treatment [11].

Research into electrochemical methods for the treatment of aqueous wastes that contain organic contaminants has focused on anodes with excellent electrochemical oxidation performance. The electrochemical activity of the anode is mainly related to the chemical composition and the structure of the coating. In past years, numerous types of metal oxide electrodes, such as SnO_2, PbO_2, IrO_2 and composite oxides, have been developed for electrochemical oxidation of organic pollutants [12-16]. It is well known that doping for these oxides coating will achieve better conductivity and more powerful electrochemical activity. Various doped metal oxide-film electrodes such as PbO_2 and SnO_2 were obtained in previous study [17,18]. SnO_2 in its pure form is a n-type semiconductor with a wide band gap (3.87-4.3 eV), which is not favorable for electron-transfer in electrochemical oxidation. Modification of SnO_2 electrode by addition of selected dopants can reduce the band gap and increase the conductivity as well as electrochemical activity. The Sb doped Ti/SnO_2 has excellent stability, conductivity and electrocatalytic activity [19,20]. To further improve the efficiency of electrochemical degradation of organic compounds on the Ti/SnO_2-Sb electrodes in the treatment process of organic wastewater, there are other attempts to dope the Ti/SnO_2-Sb electrode with other elements [21-23]. It is suggested that the enhancement of the electrode for electrochemical oxidation of organics could be attributed to the production of hydroxyl radicals. In electrochemical processes, the doping of rare earth and other metals into the film could improve the surface structure and enhance the electrode capability on mineralization of pollutant compounds. It is worthy of mention that the La and Ru species are active and are widely used as catalysts [24,25]. Recent studies indicate that a better performance is obtained for co-doped electrodes [26,27]. Some work has reported that the salicylaldehyde removal is 76.5% on Ir and Sb co-doped Ti/SnO_2 electrode after 1.5 h [28]. In another study, Ru and Ir co-doped Ti/SnO_2 electrode was prepared and phenol removal efficiency is about 99% after 8 h [29]. In this study, we selected La and Ru as co-dopant to introduce into Ti/SnO_2-Sb electrode by thermal decomposition and examined electrochemical properties of the Ti/SnO_2-Sb-La and Ti/SnO_2-Sb-Ru electrodes, and further explored the efficiency of electrochemical degradation of organic compounds using phenol as a model compound.

†To whom correspondence should be addressed.
E-mail: sun@seu.edu.cn

EXPERIMENTAL

1. Electrode Preparation

The La and Ru doped Ti/SnO_2-Sb electrodes were prepared using thermal decomposition technique. Titanium plates with dimensions of 3.0 cm×4.0 cm×0.07 cm were introduced as the base metal for all oxide-coated electrodes. Prior to coating, the Ti substrates were polished and treated in 10% boiling oxalic acid. The metal precursors were prepared using the following metal salt compounds: $SnCl_4 \cdot 5H_2O$, $SbCl_3$, $La(NO_3)_3$ and $RuCl_3$, with Sn/Sb/La (Ru) molar ratio of 100/6/2 for the doped electrodes and Sn/Sb molar ratio of 100/6 for the Ti/SnO_2-Sb. The precursor solutions were obtained by dissolution of citric acid in 5 ml ethylene glycol and 30 mL ethanol mixing solution. After ultrasonic dissolution of the citric acid, the metal precursor was added and kept under ultrasonic dissolution for 2 h. The molar ratio of the metal : citric acid : ethylene glycol was 1 : 3 : 3. The precursor solution was spread on Ti substrate, and then dried for solvent evaporation in an infrared oven at 60 °C for 30 min, and fired in a muffle oven under air at a temperature of 500 °C for 15 min. This procedure (spreading, drying and pyrolysis) was repeated 12 times and, finally, the electrodes were annealed heated at 550 °C for 3 h.

2. Characterization of Electrodes

The morphology of the electrode coating was characterized using a SEM (FEI Sirion 200). XRD patterns were used for the crystalline structure identification of the samples and obtained using a D-MAX 2200 VPC instrument with Cu K_α radiation. XPS measurements were performed on a PHI 5000 (ULVAC-PHI) system with an Al K_α source to analyze the composition and chemical state of the surface elements. All the binding energies were referenced to the C1s peak at 284.6 eV from the surface adventitious carbon.

3. Electrochemical Measurements

The coating of the electrodes was characterized by means of CV, i-t curve and EIS to evaluate electrochemical performance. All electrochemical measurements were carried out with a Zahner IM6ex electrochemical station using a three-electrode system, and the saturated calomel electrode (SCE) was used as a reference electrode. The prepared electrodes were used as the working electrode, and Ti plate was used as an auxiliary electrode. 0.1 M KCl solution containing 5 mM $K_4[Fe(CN)_6]$ was used for CVs measurement. The EIS and i-t curve were measured in 500 mg L^{-1} phenol solution containing 0.1 M Na_2SO_4 as the supporting electrolyte. The accelerated lifetime was measured in the 1 M H_2SO_4 solution at 40 °C with a constant anodic current density of 2 A cm^{-2}. The working electrodes were the prepared anodes, and stainless steel was used as a counter electrode. The accelerated life of an electrode was defined as the operation time when bath voltage between working and counter electrode increases by 5 V compared with the initial voltage.

4. Electrochemical Treatment

The electrochemical degradation of organic pollutants was carried out in a single-compartment cell equipped with a magnetic stirrer. The fabricated electrodes (the same surface area) served as the anodes and a Ti plate with the same area as a cathode, and the distance between the anode and cathode was 15 mm. 100 mL wastewater containing 500 mg L^{-1} phenol and 0.1 M Na_2SO_4 was charged in an electrolysis cell. The operating current density was 30 mA cm^2. The concentration of phenol was monitored by HPLC during electrochemical oxidation process, which was carried out on a Perkin Elmer Series 200 LC at 25 °C. Chromatographic separation was performed using an ODS-18 reversed phase column (250 mm×4.6 mm, 5 μm), and the mobile phase consisted of methanol/water (40/60, v/v) at a flow rate of 1 mL min^{-1}, and 15 μL of sample was injected. The UV detector was set at 275 nm. COD was measured with the standard potassium dichromate method (China GB11914-89). The phenol solution was sampled at each 30 min interval for COD measurement. 0.5 mL of solution sample was diluted. COD was measured by a titrimetric method after the sample was digested using dichromate as the oxidant in acidic solution at 150 °C for 2 h. The UV absorption spectroscopy was recorded from 200 to 400 nm using a Shimadzu UV-2450 spectrophotometer.

RESULTS AND DISCUSSION

1. Characteristics of the Electrodes

The surface morphology of the electrode coating mainly depends on the composition of the precursor solution and the conditions of preparation. Fig. 1 shows the SEM microstructures of the Ti/SnO_2-Sb-La, Ti/SnO_2-Sb-Ru and the Ti/SnO_2-Sb electrodes. As shown in Fig. 1(a), the coating particles of the Ti/SnO_2-Sb electrode are uniform in size with diameters ranging from 50 to 100 nm. Fig. 1(b)

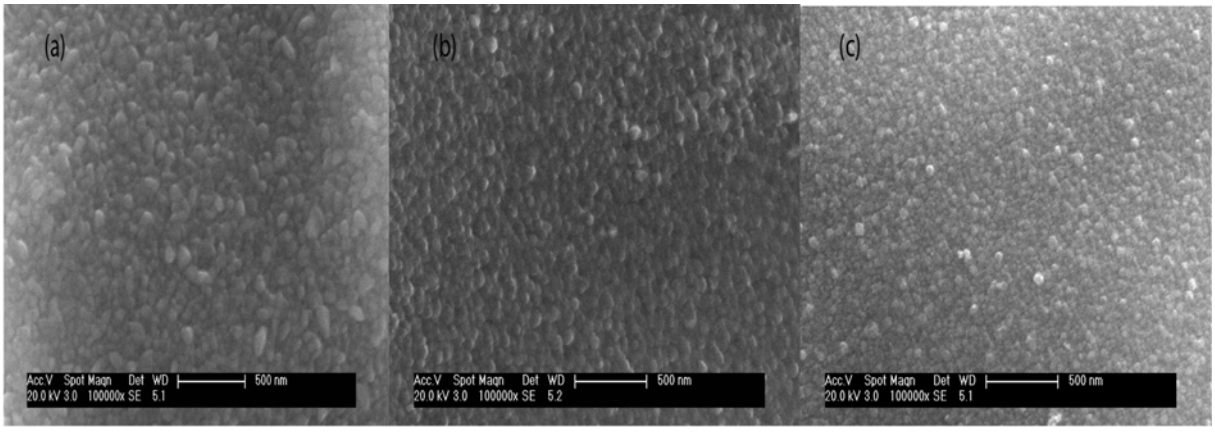

Fig. 1. SEM surface images of the Ti/SnO_2-Sb (a), Ti/SnO_2-Sb-Ru (b) and Ti/SnO_2-Sb-La (c) electrodes.

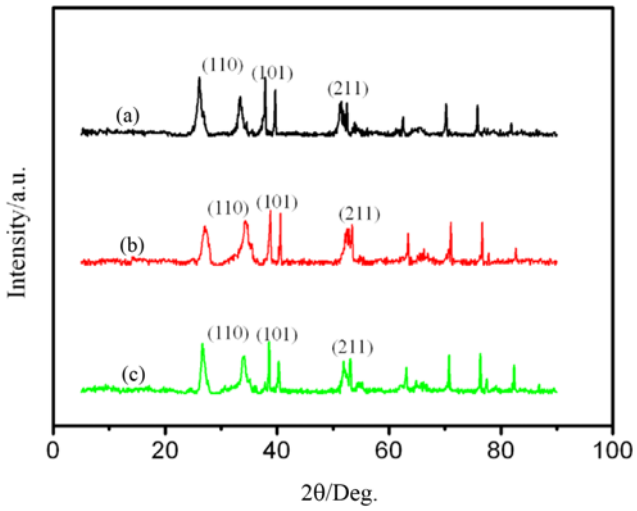

Fig. 2. XRD patterns of the Ti/SnO_2-Sb-La (a), Ti/SnO_2-Sb-Ru (b) and Ti/SnO_2-Sb (c) electrodes.

and (c) show the surface morphology of the Ti/SnO_2-Sb-Ru and Ti/SnO_2-Sb-La electrode coatings. The nanoparticles dispersed regularly on the surface of the Ti substrates, with sizes of about 30-50 nm and 20-40 nm for the Ti/SnO_2-Sb-Ru and Ti/SnO_2-Sb-La electrodes. Particle sizes of the La and Ru doped electrodes become smaller than that of the SnO_2-Sb electrode, having larger surface areas, and could provide more active sites for electrochemical oxidation.

Fig. 2 records the XRD patterns of the Ti/SnO_2-Sb-La, Ti/SnO_2-Sb-Ru and the Ti/SnO_2-Sb electrodes, which only show a series of diffraction peaks of the SnO_2 structure and metal Ti substrate. No diffraction peak of La, Ru or Sb metal oxide was clearly found from the XRD spectra. The peaks corresponding to $2\theta \approx 26.7^\circ$, 33.8° and 51.9° were assigned to the (110), (101) and (211) planes of SnO_2. The peak positions agreed well with the reflections of SnO_2, indicating a tetragonal rutile structure. The average values of the lattice parameters can be calculated for the different electrodes by Bragg's formula [30] according to the XRD patterns (Table 1). The lattice parameters of SnO_2 with the Ru doped electrode (a=b=4.702 Å, c=3.170 Å) were lower than those of the Ti/SnO_2-Sb electrode (a=b=4.718 Å, c=3.176 Å). However, the SnO_2 lattice was expanded with La doped electrodes (a=b=4.738 Å, c=3.182 Å) compared with the Ti/SnO_2-Sb electrode. A reasonable explanation for the lattice deformation was that the larger La ions and the smaller Ru ions replaced the Sn^{4+} ions in the unit cell of the SnO_2. The average crystallite size of SnO_2 (the (110) plane, $2\theta \approx 26.7^\circ$) was estimated using the Scherrer equation [31]. The average crystallite size is mainly concerned with the preparation technique (such as annealed tem-

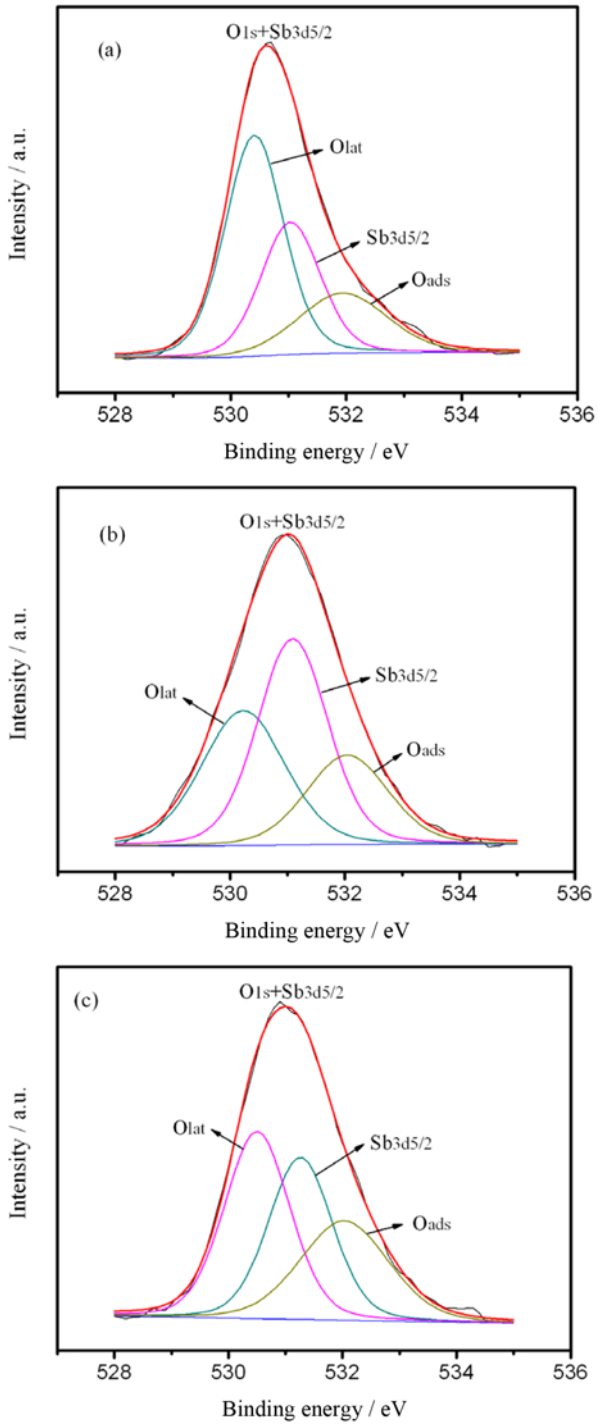

Fig. 3. Fitted curves of O1s and $Sb3d_{5/2}$ XPS spectra on the coating film surfaces of the Ti/SnO_2-Sb (a), Ti/SnO_2-Sb-Ru (b) and Ti/SnO_2-Sb-La (c) electrodes.

Table 1. Refinements to the XRD patterns of SnO_2 on the different electrodes

Sample	Cation radius (Å)		Average crystallite size (nm)	Lattice parameters (Å)	
	Sn^{4+}	Doping cation		a(b)	c
Ti/SnO_2-Sb	0.71		12.0	4.718	3.176
Ti/SnO_2-Sb-Ru	0.71	0.64 (Ru^{4+})	9.7	4.702	3.170
Ti/SnO_2-Sb-La	0.71	1.06 (La^{3+})	8.6	4.738	3.182

Table 2. XPS analysis on the surfaces of the Ti/SnO_2-Sb, Ti/SnO_2-Sb-Ru and Ti/ SnO_2-Sb-La electrodes

Sample	Binding energy/eV				O_{ads} content/%	O_{lat} content/%
	Sn $3d_{5/2}$	Sb $3d_{5/2}$	O1s (ads)	O1s (lat)		
Ti/SnO_2-Sb	486.71	530.99	531.86	530.36	29.13	70.87
Ti/SnO_2-Sb-Ru	486.66	530.94	531.89	530.08	39.42	60.58
Ti/SnO_2-Sb-La	486.73	531.12	531.89	530.36	41.78	58.22

perature, annealed time, dopant and so on), which will increase with the sintering temperature and time [32]. The average crystallite sizes of SnO_2 were about 12.0, 9.7 and 8.6 nm for the Ti/SnO_2-Sb, Ti/SnO_2-Sb-Ru and Ti/SnO_2-Sb-La electrodes, respectively. The decrease of the crystallite size can be ascribed as the growth of the crystal phase is hindered by the high distortion effects owing to La and Ru doping in the lattice shape. Smaller crystallite size is favorable to improve electrochemical activity of the electrode.

XPS measurements of the electrodes were made to analyze the surface compositions and element chemical states of the electrodes. The XPS spectra confirmed the existence of Sn^{4+}, Sb^{5+}, La^{3+} and Ru^{4+}. The XPS investigations were focused mainly on the detailed analysis of O elements. The XPS spectra of Sb $3d_{5/2}$ and O1s are overlapped. They were fitted using XPS Peak Fitting Program as shown in Fig. 3. The mixed spectra (Sb$3d_{5/2}$ plus O1s) were fitted into three peaks, which correspond to different species, and the deconvoluted values are given in Table 2. The binding energy (BE) of Sb$3d_{5/2}$ was around 531.0 eV for all of the samples, in agreement with other researchers for Sb^{5+} [33]. Two O1s peaks appeared after deconvolution. A lower BE component peak with the BE values at about 530.08-530.36 eV and a higher component peak at about 531.86-531.89 eV could be observed. The lower BE peak is assigned to the lattice oxygen O_{lat} which are incorporated into SnO_2 crystal lattice, and the higher BE peak may be ascribed to adsorbed oxygen species O_{ads} which are adsorptive O_2 and/or weakly bonded oxygen species (e.g., hydroxyl group) [34,35]. The relative content of different kinds of oxygen species could be calculated by the XPS peak area ratio due to the same sensitivity factors for O_{ads} and O_{lat}. Table 2 shows the content of different chemical states of the O element on the surface of the different electrodes. O_{ads} content on the surface of the Ti/SnO_2-Sb-La electrode is the highest. It is 41.78% for the Ti/SnO_2-Sb-La electrode, 39.42% for the Ti/SnO_2-Sb-Ru electrode and 29.13% for the Ti/SnO_2-Sb electrode. The O_{ads} is the most active oxygen species and plays an important role in oxidation process [36]. Electrochemical oxidation of organic compounds could proceed as follows [37,38]:

$$MO_x(\cdot OH) \rightarrow MO_{x+1} + H^+ + e^- \quad (1)$$

$$R + MO_x(\cdot OH) \rightarrow CO_2 + MO_x + zH^+ + ze^- \quad (2)$$

$$R + MO_{x+1} \rightarrow MO_x + RO \quad (3)$$

The first step is the oxidation of water molecules on the electrode surface (MO_x), giving rise to formation of physisorbed hydroxyl radicals ($MO_x(\cdot OH)$, O_{ads}). $MO_x(\cdot OH)$ can oxidize the crystal lattice of MO_x to a higher state forming higher oxide MO_{x+1}. The physisorbed hydroxyl radicals ($MO_x(\cdot OH)$, O_{ads}), because of their high reactivity toward most organic compounds, are readily reacting with organic substrates close to anode surface to form carbon dioxide and water. For the Ti/SnO_2-Sb-La and Ti/SnO_2-Sb-Ru electrodes, the amount of adsorbed O_{ads} on the surface is more than that of the Ti/SnO_2-Sb electrode. Therefore, reaction 2 occurs much more easily compared with reaction 3. The increasing of the O_{ads} implied that the electrochemical activity of the Ti/SnO_2-Sb anode would be considerably affected by La and Ru doping.

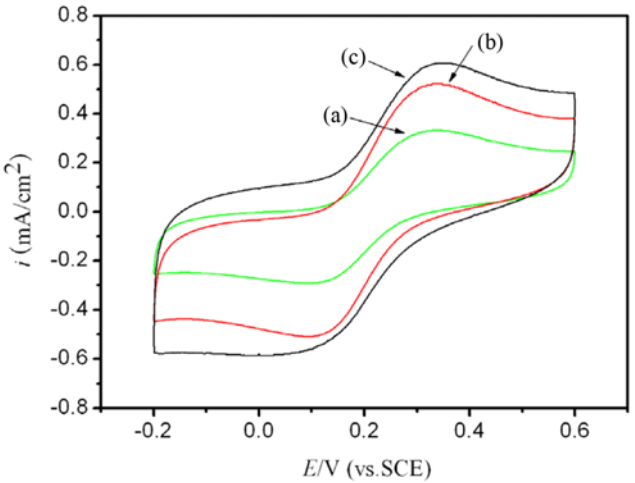

Fig. 4. CVs obtained with the Ti/SnO_2-Sb (a), the Ti/SnO_2-Sb-Ru (b) and the Ti/SnO_2-Sb-La (c) electrodes in 0.1 M KCl solution containing 5 mM $K_4[Fe(CN)_6]$ at a scan rate of 100 mV s^{-1}.

2. Electrochemical Measurements

CVs were used to evaluate electrochemical performance of the electrode surface. The $Fe(CN)_6^{3-/4-}$ redox couple, involving outer-sphere electron transfer, was widely used as an electrochemical probe in the electrochemical study [39]. Fig. 4 shows the voltammograms of the three electrode systems at a scan rate of 100 mV s^{-1}. In this potential region the observed voltammetric current is the sum of the electrode surface redox transitions and the double layer charging [40]. Anodic current peak and cathodic current peak corresponding to $Fe(CN)_6^{3-/4-}$ redox transition are observed at about 0.35 V and 0.1 V versus SCE, respectively. The value of DEp (about 250 mV) is consistent with the literature [21]. The values of DEp for the $Fe(CN)_6^{3-/4-}$ couple had not been reduced by the presence of the codopants, but an increase of the anodic peak current densities (i_p) is observed for the co-doped electrodes. The values of i_p were 0.60, 0.52 and 0.37 mA cm^{-2} for the Ti/SnO_2-Sb-La, Ti/SnO_2-Sb-Ru and the Ti/SnO_2-Sb electrodes, respectively. This indicated that the La and Ru doped coatings effectively enhance the electron transfer from ferricyanide to the electrode. Moreover, integration of the i–E curve provides the voltammetric charge, which is proportional to the number of electrochemically surface active sites [41]. CV scans showed that

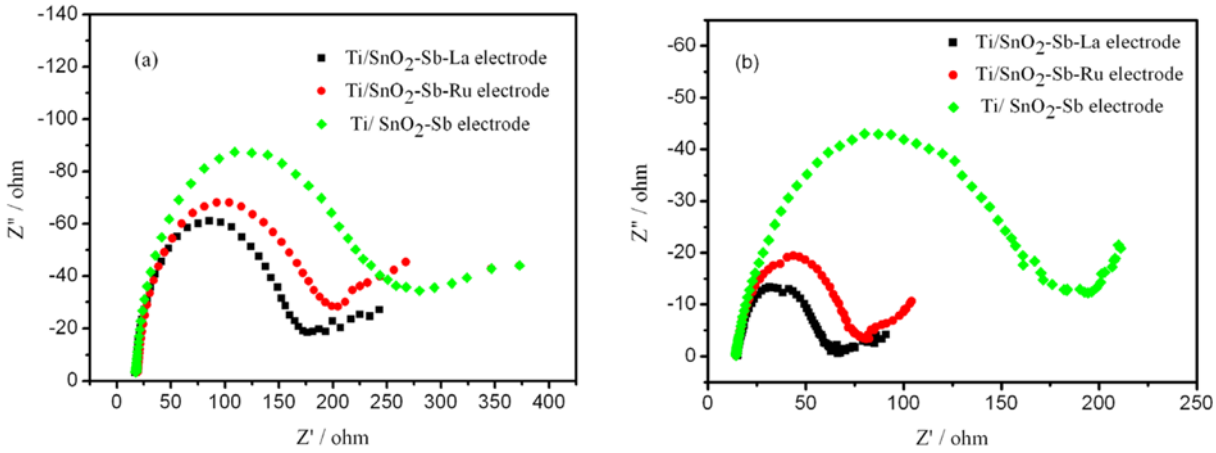

Fig. 5. EIS Nyquist plots of the Ti/SnO_2-Sb, Ti/ SnO_2-Sb-Ru and the Ti/SnO_2-Sb-La electrodes in 0.1 M Na_2SO_4 solution (a) and 0.1 M Na_2SO_4 solution containing 500 mg L^{-1} phenol (b) under a bias potential of 3 V vs SCE.

the voltammetric charges on the Ti/SnO_2-Sb-La electrode and the Ti/SnO_2-Sb-Ru electrode were more than on the Ti/SnO_2-Sb electrode, which is attributed to the increase of whole active surface of the Ti/SnO_2-Sb-La electrode and the Ti/SnO_2-Sb-Ru electrode. This is also in good agreement with the results from SEM and XRD.

It was an effective approach to study the interfacial properties of the doped electrode by EIS spectra. Fig. 5 shows EIS Nyquist plots of the three electrodes, which were recorded between 100 kHz and 10 mHz with the amplitude of the ac signal 5 mV at 3 V. The Nyquist plots for the three electrodes are almost similar in form, composed of a depressed semicircle shape at medium-high frequency and an approximate straight line at low frequency. The medium-high-frequency semicircle is ascribed to the process at the coating/electrolyte interface, which is expected to be the double-layer capacitance (CPE, the constant phase element) in parallel with the charge-transfer impedance (R_{ct}) due to the charge exchange and compensation at the coating/solution interface [42-44]. The EIS data analysis was performed using ZView software. Table 3 shows the R_{ct} values of the three electrodes. The Ti/SnO_2-Sb electrode presents the largest R_{ct} value due to its low conductivity for charge transfer between the electrode surface and the solution. The R_{ct} values on the Ti/SnO_2-Sb-La electrode (155.3 Ω) and Ti/SnO_2-Sb-Ru electrode (175.4 Ω) were less than that of the Ti/SnO_2-Sb electrode (226.9 Ω), mainly due to the superior conductivity of La and Ru doped. After addition of phenol to the solution, the R_{ct} values of the Ti/SnO_2-Sb, Ti/SnO_2-Sb-Ru and Ti/SnO_2-Sb-La electrodes were 145.1, 60.3 and 44.6 Ω, respectively. The decrease of R_{ct} can be attributed to the electrochemical oxidation of phenol on the electrodes. The R_{ct} decrease on the Ti/SnO_2-Sb-Ru electrode and the Ti/SnO_2-Sb-La electrode was more than that of the Ti/SnO_2-Sb electrode, indicating its better electrochemical capacity for phenol oxidation.

Accelerated lifetime tests were carried out with the three electrodes. The electrolysis time when bath voltage increases by 5 V compared with the initial voltage was regarded as the accelerated lifetime of the anode. Accelerated lifetime tests showed that the lifetimes of the Ti/SnO_2-Sb, Ti/SnO_2-Sb-Ru and Ti/SnO_2-Sb-La electrodes were 28.5, 34.0 and 35.5 h, respectively (Table 2). A sharp potential increase was observed during the last few hours. It is indicated that the coating would be eroded and an insulator rutile TiO_2 film would be generated on the interface of Ti-substrate and the coating [45]. The lifetimes of the Ti/SnO_2-Sb-Ru and Ti/SnO_2-Sb-La electrodes have been enhanced due to good bonding between the coating and the Ti substrate. This can be explained by a smaller residual mechanical stress of thermal expansion between the coating and the base metal due to lower impedance of the Ru or La doped Ti/SnO_2-Sb electrode.

Further concern focuses on the electrochemical property of the three electrodes, which was studied through the current density versus time (i-t) curve under 3.0 V in a 0.1 M Na_2SO_4 solution with 500 mg L^{-1} phenol. Table 3 shows the evolution of the current densities on the three electrodes. It can be seen that the current densities of the Ti/SnO_2-Sb, Ti/SnO_2-Sb-Ru and Ti/SnO_2-Sb-La electrodes are 12.6, 15.7 and 16.9 mA cm^{-2}, respectively. The current density of Ti/SnO_2-Sb-La is the maximum. The current densities of the three

Table 3. Parameters of the Ti/SnO_2-Sb, Ti/SnO_2-Sb-Ru and Ti/SnO_2-Sb-La electrodes

	Ti/SnO_2-Sb	Ti/SnO_2-Sb-Ru	Ti/SnO_2-Sb-La
Electron transfer resistance without phenol (R_{ct}/Ω)	226.9	175.4	155.3
Electron transfer resistance with phenol (R_{ct}/Ω)	145.1	60.3	44.6
R_{ct} decrease (Ω)	81.8	115.1	110.7
Current density without phenol (mA cm^{-2})	12.6	15.7	16.9
Current density with phenol (mA cm^{-2})	16.7	22.5	24.3
Current density increase (mA cm^{-2})	4.1	6.8	7.4
Accelerated lifetime (h)	28.5	34.0	35.5

electrodes are all increased after addition of phenol to the solution. On Ti/SnO_2-Sb-Ru, the current density increases to 22.5 mA cm^{-2}, with a 43.3% increment. On Ti/SnO_2-Sb-La, the current density increases to 24.3 mA cm^{-2}, with a 43.8% increment. In contrast, on Ti/SnO_2-Sb, the current density increases to 16.7 mA cm^{-2}, with a lower increment of 32.5%. The increase of the current density can be attributed to the electrochemical oxidation of phenol on the electrodes. The current density increase on Ti/SnO_2-Sb-La and Ti/SnO_2-Sb-Ru is higher than that of Ti/SnO_2-Sb. This can be partially ascribed to the larger surface area, which provides multiple nanostructures and more exposed active sites for adsorbed •OH and organic compounds. The large quantity of adsorbed •OH accelerates the oxidation of organic compounds.

3. Electrochemical Oxidation of Phenol

Three different electrodes were tested as the anode in electrochemical degradation of phenol to further evaluate the effect of the La and Ru doping for electrochemical oxidation. As Fig. 6(a) shows, a steep decrease for phenol concentration with the three electrodes was obtained in electrolysis reaction time of 1 h, but phenol removal was obviously faster on the Ti/SnO_2-Sb-La and Ti/SnO_2-Sb-Ru than on the Ti/SnO_2-Sb electrode. Phenol is almost converted on the Ti/SnO_2-Sb-La electrode at 2 h, with the removal of 99.3%. At the same time, the phenol removal on the Ti/SnO_2-Sb-Ru electrode is 95.8%, but only a removal of 83.6% on the Ti/SnO_2-Sb electrode. The observed rates of phenol degradation were fitted with pseudo-first-order rate constants (Fig. 6(b)). The apparent rate constant (k) on Ti/SnO_2-Sb electrode is 0.018 min^{-1}. The k values on the Ti/SnO_2-Sb-Ru and Ti/SnO_2-Sb-La electrode are 0.038 and 0.050 min^{-1}, which are 2.1 and 2.8 times that of the Ti/SnO_2-Sb electrode, respectively.

The COD removal of phenol on the three electrodes is shown in Fig. 6(c). The COD removed was higher on the Ti/SnO_2-Sb-La and Ti/SnO_2-Sb-Ru electrodes than that on the Ti/SnO_2-Sb electrode. At 2.5 h, the COD removal is 86.4%, 82.1% and 60.2% on Ti/SnO_2-Sb-La, Ti/SnO_2-Sb-Ru and Ti/SnO_2-Sb, respectively. The rates of COD removal were fitted with pseudo-first-order rate constants (Fig. 6(d)), and the k values are 0.0063, 0.0123, and 0.0133 min^{-1} on the Ti/SnO_2-Sb, Ti/SnO_2-Sb-Ru and Ti/SnO_2-Sb-La electrodes, respectively. Additionally, the current efficiency (CE) was calculated based on the following equation [46]:

$$CE(\%) = \frac{(COD_0 - COD_t)}{8It} FV \times 100 \quad (4)$$

where COD_0 and COD_t are the COD (in g of O_2 dm^{-3}) at times 0 and t (s), respectively, F is Faraday's constant (96,487 C mol^{-1}), V is the volume of the electrolyte (dm^3), I is the current (A), and 8 is the equivalent mass of oxygen (g eq^{-1}).The CEs are 40.65%, 38.63%

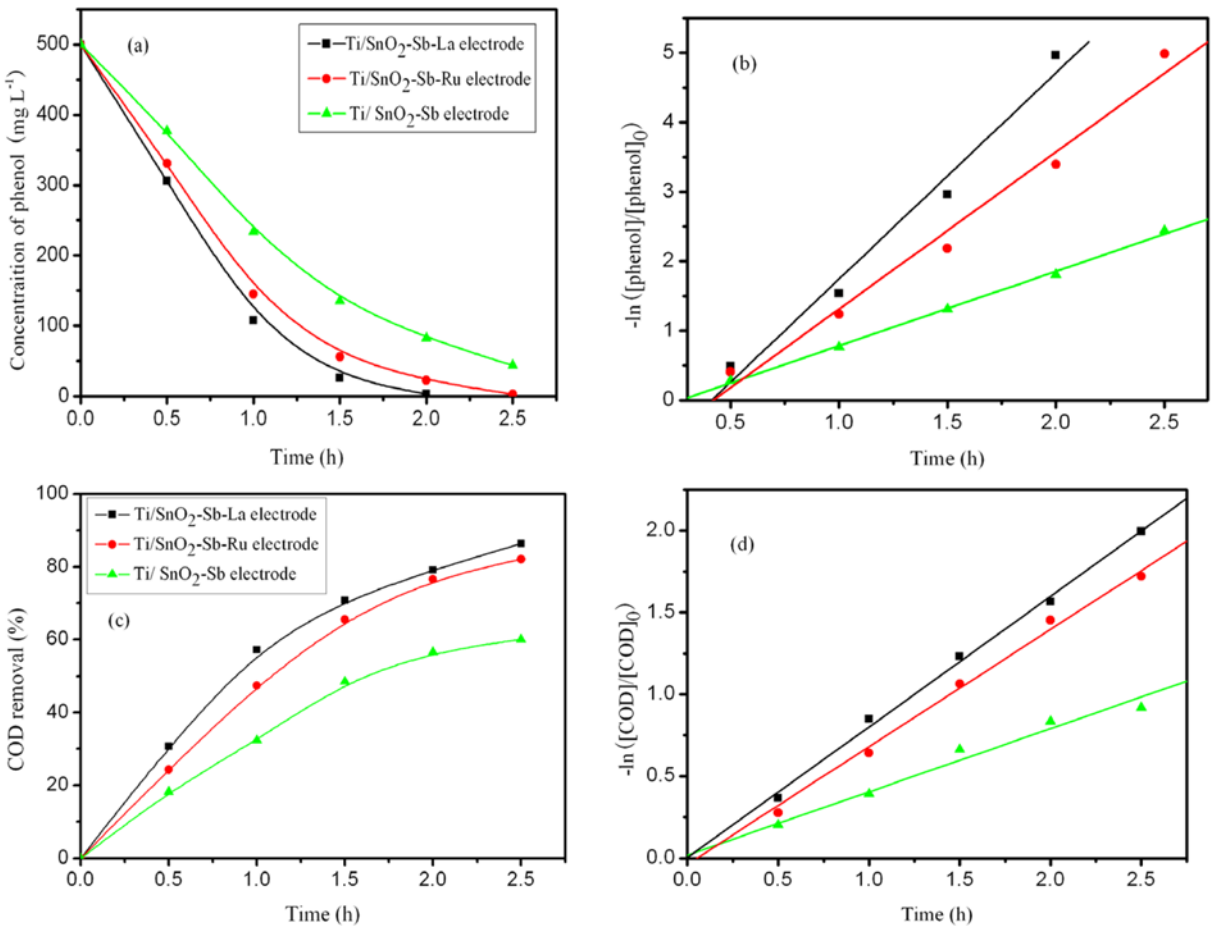

Fig. 6. Comparison of phenol oxidation on the Ti/SnO_2-Sb-La, Ti/SnO_2-Sb-Ru and Ti/SnO_2-Sb electrodes in 500 mg L^{-1} phenol and 0.1 M Na_2SO_4 solution with current density 30 mA cm^{-2}. (a) phenol concentration changes with time, (b) the apparent rate constant of phenol degradation, (c) COD removal changes with time, (d) the apparent rate constant of COD removal.

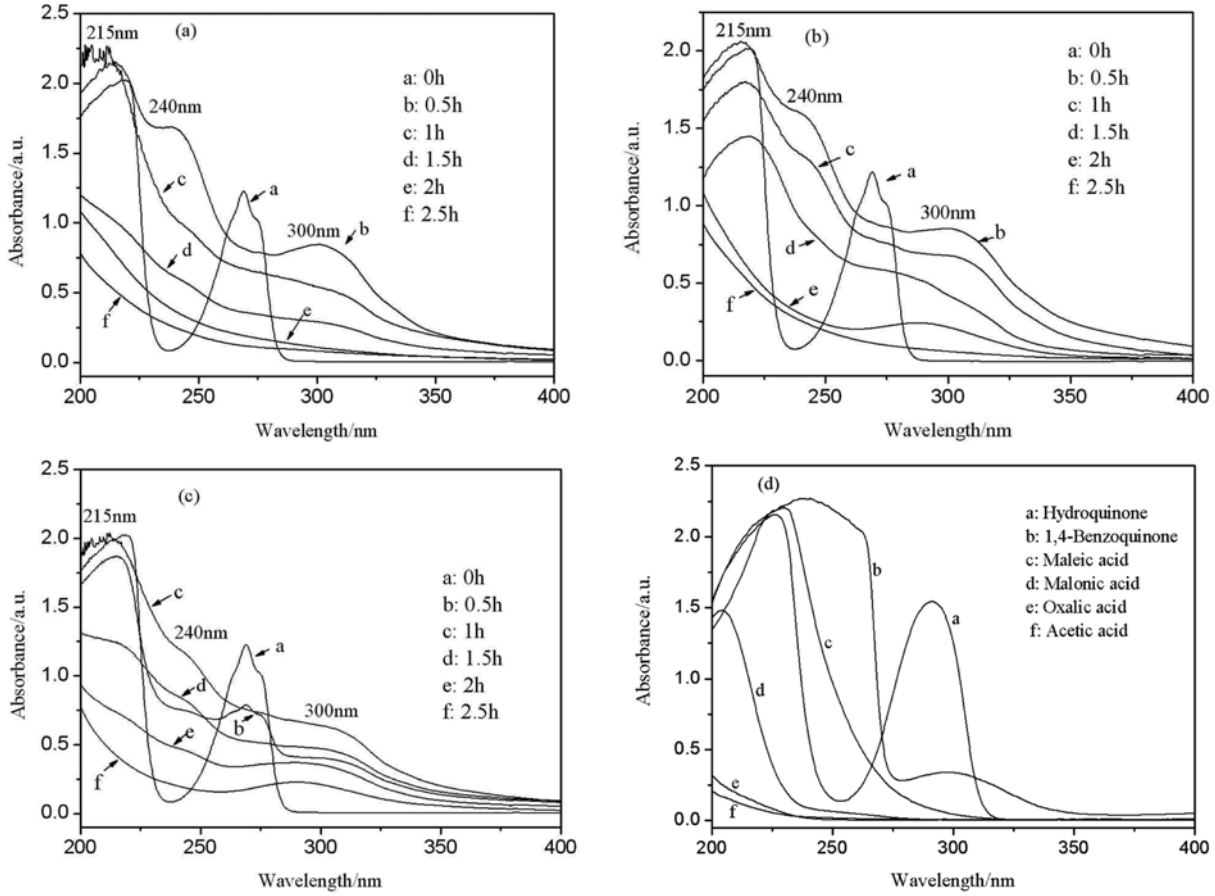

Fig. 7. UV spectra of the phenol solution as a function of electrolysis time with the Ti/SnO_2-Sb-La (a), Ti/SnO_2-Sb-Ru (b) and Ti/SnO_2-Sb (c) electrodes; (d) UV spectra of some possible intermediates.

and 28.29% in 2.5 h for the Ti/SnO_2-Sb-La, Ti/SnO_2-Sb-Ru and Ti/SnO_2-Sb electrodes. The La and Ru doped electrodes showed higher electrochemical oxidation capacity.

Fig. 7 shows the UV scans (200-400 nm) of the electrolytes obtained during the electrolysis process, and the fabricated electrodes were used as anode. Electrochemical activation of the anodes and possible intermediates formed in the phenol oxidation process could be evaluated. The mechanism of electrochemical oxidation of phenol has been shown in previous research as the following [27,47,48]: (i) oxidation of phenol to other hydroxylated or oxygenated compounds, especially quinonic compounds (cyclic intermediates), (ii) the ring opening reaction to form aliphatic acids, and (iii) mineralization of the aliphatic acids to carbon dioxide and H_2O. Fig. 7(a) shows that phenol decreased dramatically with the Ti/SnO_2-Sb-La electrode along the reaction time. The peak at about 270 nm represents the presence of the aromatic ring of phenol. The new peaks at about 240 and 300 nm synchronously appeared for 0.5 h electrolysis, which might represent the formation of two intermediates, hydroquinone and benzoquinone. After 1 h electrolysis, the absorbance peaks at 240 and 300 nm decreased and the peaks at 200-215 nm simultaneously increased, which indicated that the ring of aromatic compounds is fractured to form carboxylic acids. After 2.5 h electrolysis, the peaks at 240 and 300 nm disappeared completely, suggesting hydroquinone and benzoquinone was entirely destroyed. For the Ti/SnO_2-Sb-La electrode, the aromatic ring cleavage is comparatively rapid, with very little accumulation of hydroquinone and benzoquinone. With continuous electrolysis, more carboxylic acids, as intermediates, were eventually mineralized to come into CO_2 and H_2O. These results show that high efficiency is obtained with Ti/SnO_2-Sb-La electrode for phenol oxidation to benzoquinone and benzoquinone oxidation, which is related to the aromatic rings opening.

As Fig. 7(b) shows, similar electrochemical degradation processes of phenol were obtained for the Ti/SnO_2-Sb-Ru anode. However, on the Ti/SnO_2-Sb electrode (Fig. 7(c)), the peak at 300 nm did not disappear at 2.5 h, indicating the partial oxidation of hydroquinone and benzoquinone. This illuminates that the cleavage of aromatic ring takes place more easily on the Ti/SnO_2-Sb-La and Ti/SnO_2-Sb-Ru electrodes than that on the Ti/SnO_2-Sb electrode. The removal of substrate and the cleavage of aromatic rings affected the ultimate mineralization efficiency to a certain degree. UV spectral analysis shows that the degradation efficiency of phenol was highest on the La-doped electrode and lowest on the Ti/SnO_2-Sb electrode under the same condition, which is consistent with the aforementioned results obtained by COD and phenol concentration records.

Electrochemical oxidation of many organic pollutants on anode could take place by electron transfer and active reactant. Electrochemical oxidation could proceed through several steps, such as mass transport, adsorption and direct or indirect reaction at the anode surface. Direct or indirect reaction can be considered as electrochemi-

cal conversion and electrochemical combustion [49]. The active sites of the La and Ru doped Ti/SnO_2-Sb electrode increase, and the charge-transfer resistance of the electrode/solution interface is reduced. The introduction of La and Ru strengthens the capacity of physical adsorption for hydroxyl radicals on the electrode surfaces. Those lead to a quantitative increase of hydroxyl radicals (O_{ads}) on the electrode surface. When organic compounds came close to electrode/solution interface, oxidation reaction with adsorbed hydroxyl radicals occurred easily. Complete combustion of organic compounds is more on the surfaces of the Ti/SnO_2-Sb-La and Ti/SnO_2-Sb-Ru electrodes due to O_{ads} than that on the Ti/SnO_2-Sb and so the degradation of phenol is of relatively high efficiency.

CONCLUSION

The doping of La and Ru affected the electrochemical performance of Ti/SnO_2-Sb electrode and improved the effect of phenol degradation. The results of this study revealed the following:

• Crystallite sizes of the coating became smaller on the Ti/SnO_2-Sb-La and Ti/SnO_2-Sb-Ru than that on the Ti/SnO_2-Sb due to La and Ru doping. The electroactive surface area of the doped electrodes was increased. The electronic conducting performance of the doped electrodes was enhanced and accompanied by an improvement of electrochemical properties of the electrodes.

• The rates of COD removal and phenol elimination were the highest on the Ti/SnO_2-Sb-La electrode and were the lowest on the Ti/SnO_2-Sb electrode.

• La and Ru doped in the coating of the electrode enhanced the capacity of physical adsorption for hydroxyl radicals (O_{ads}), which led to improved effectiveness on phenol degradation.

ACKNOWLEDGEMENTS

Authors thank the National Natural Science Fund Committee (21173042), Jiangsu Natural Science Foundation (BK2011589), Key Laboratory for Attapulgite Science and Applied Technology of Jiangsu Province and State Key Laboratory of Silicon Materials visiting scholar Fund (SKL2011-17), Laboratory Management and Research Program of Southeast University (2010-L017).

REFERENCES

1. M. A. Maluleke and V. M. Linkov, *Sep. Purif. Technol.*, **32**, 377 (2003).
2. R. Levi, M. Milman, M. V. Landau, A. Brenner and M. Herskowitz, *Environ. Sci. Technol*., **42**, 5165 (2008).
3. S. Hammami, N. Oturan, N. Bellakhal, M. Dachraoui and A. M. Oturan, *J. Electroanal. Chem.*, **610**, 75 (2007).
4. T. C. An, X. H. Zhu and Y. Xiong, *Chemosphere*, **46**, 897 (2002).
5. Y. Lee, Y. Kim, H. Jeong, M. K.Yeo and M. Kang, *Bull. Korean Chem. Soc.*, **30**, 107 (2009).
6. S. M. Lam, J. C. Sin and A. R. Mohamed, *Korean J. Chem. Eng.*, **27**, 1109 (2010).
7. J. H. Park, Y. S. Seo, H. S. Kim and I. K. Kim, *Korean J. Chem. Eng.*, **28**, 1693 (2011).
8. L. Szpyrkowicz, S. N. Kaul, R. N. Neti and S. Satyanarayan, *Water Res.*, **39**, 1601 (2005).
9. M. Panizza, M. Delucchi and G. Cerisola, *J. Appl. Electrochem.*, **35**, 357 (2005).
10. P. Cañizares, J. A. Domínguez, M. A. Rodrigo, J. Villaseñor and J. Rodríguez, *Ind. Eng. Chem. Res.*, **38**, 3779 (1999).
11. Y. Xiong, C. He, H. T. Karlsson and X. H. Zhu, *Chemosphere*, **50**, 131 (2003).
12. O. Simond and C. Comninellis, *Electrochim. Acra*, **42**, 2013 (1997).
13. H. C. Ma, C. P. Liu, J. H. Liao, Y. Su, X. Z. Xue and W. Xing, *J. Mol. Catal. A: Chem.*, **247**, 7 (2006).
14. M. Vuković, D. Marijan, D. Čukman, P. Pervan and M. Milun, *J. Mater. Sci.*, **34**, 869 (1999).
15. C. Comninellis and G. P. Vercesi, *J. Appl. Electrochem.*, **21**, 335 (1991).
16. P. Duverneuil, F. Maury, N. Pebere, F. Senocq and H. Vergnes, *Surf. Coat. Technol.*, **151-152**, 9 (2002).
17. C. L. P. S. Zanta, P. A. Michaud, C. Comninellis, A. R. De Andrade and J. F. C. Boodts, *J. Appl. Electrochem.*, **33**, 1211 (2003).
18. C. R. Costa, C. M. R. Botta, E. L. G. Espindola and P. Olivi, *J. Hazard. Mater.*, **153**, 616 (2008).
19. B. Hadjarab, A. Bouguelia, A. Benchettara and M. Trari, *J. Alloy. Compd.*, **461**, 360 (2008).
20. L. Lipp and D. Pletcher, *Electrochim. Acta*, **42**, 1091 (1997).
21. B. Correa-Lozano, C. Comninellis and A. D. De-Battisti, *J. Appl. Electrochem.*, **26**, 683 (1996).
22. L. L. Houk, S. K. Johnson, J. Feng, R. S. Houk and D. C. Johnson, *J. Appl. Electrochem.*, **28**, 1167n (1998).
23. Y. H. Wang, K. Y. Chan, X. Y. Li and S. K. So, *Chemosphere*, **65**, 1087 (2006).
24. S. K. Johnson, L. L. Houk, J. R. Feng, R. S. Houk and D. C. Johnson, *Environ. Sci. Technol.*, **33**, 2638 (1999).
25. M. E. Makgae, C. C. Theron, W. J. Przybylowicz and A. M. Crouch, *Mater. Chem. Phys.*, **92**, 559 (2005).
26. Y. J. Feng, Y. H. Cui, L. Bruce and Z. q. Liu, *Chemosphere*, **70**, 1629 (2008).
27. S. Ardizzone, C. L. Bianchi, G. Cappelletti, M. Ionita, A. Minguzzi, S. Rondinini and A. Vertova, *J. Electroanal. Chem.*, **589** 160 (2006).
28. N. Matyasovszky, M. Tian and A. Chen, *J. Phys. Chem. A*, **113**, 9348 (2009).
29. M. E. Makgae, M. J. Klink and A. M. Crouch, *Appl. Catal. B: Environ.*, **84**, 659 (2008).
30. F. Montilla, E. Morallon, A. De Battisti, S. Barison, S. Daolio and J. L. Vazquez, *J. Phys. Chem. B*, **108**, 15976 (2004).
31. A. Weibel, R. Bouchet, F. Boulc'h and P. Knauth, *Chem. Mater.*, **17**, 2378 (2005).
32. G. E. S. Brito, S. H. Pulcinelli and C. V. Santilli, *J. Mater. Sci.*, **31**, 4087 (1996).
33. B. Correalozano, C. Comninellis and A. De Battisti, *J. Electrochem. Soc.*, **143**, 203 (1996).
34. B. M. Trost, C. Chan and G. Ruhter, *J. Am. Chem. Soc.*, **109**, 3486 (1987).
35. K. Srinivas, M. Vithal, B. Sreedhar, M. M. Raja and P. V. Reddy, *J. Phys. Chem. C*, **113**, 3543 (2009).
36. S. Yang, Y. Feng, J. Wan, W. Zhu and Z. Jiang, *Appl. Surf. Sci.*, **246**, 222 (2005).
37. S. Fierro, T. Nagel, H. Baltruschat and C. Comninellis, *Electrochem. Commun.*, **9**, 1969 (2007).
38. C. Mousty, G. Fóti, Ch. Comninellis and V. Reid, *Electrochim. Acta*,

45, 451 (1999).
39. J. Li, A. Cassell, L. Delzeit, J. Han and M. Meyyappan, *J. Phys. Chem. B*, **106**, 9299 (2002).
40. C. L. P. S. Zanta, A. R. De Andrade and J. F. C. Boodts, *J. Appl. Electrochem.*, **30**, 467 (2000).
41. D. T. Cestarolli and A. R. De Andrade, *Electrochim. Acta*, **48**, 4137 (2003).
42. Q. F. Yi, W. Huang, J. J. Zhang, X. P. Liu and L. Li, *J. Electroanal. Chem.*, **610**, 163 (2007).
43. E. Rasten, G. Hagen and R. Tunold, *Electrochim. Acta*, **48**, 3945 (2003).
44. C. Karunakaran, P. Gomathisankar and G. Manikandan, *Korean J. Chem. Eng.*, **28**, 1214 (2011).
45. Z. G. Ye, H. M. Meng, D. Chen, H. Y. Yu, Z. S. Huan, X. D. Wang and D. B. Sun, *Solid State Sci.*, **10,** 346 (2008).
46. X. P. Zhu, S. Y. Shi, J. J. Wei, F. X. Lv, H. Z. Zhao, J. T. Kong, Q. He and J. N. Ni, *Environ. Sci. Technol.*, **41**, 6541 (2007).
47. O. Chailapakul, E. Popa, H. Tai, B. V. Sarada and D. A. Tryk, *Electrochem. Commun.*, **2**, 422 (2000).
48. H. J. Jung, J. S. Hong and J. K. Suh, *Korean J. Chem. Eng.*, **28**, 1882 (2011).
49. S. Fierro, T. Nagel, H. Baltruschat and C. Comninellis, *Electrochem. Commun.*, **9**, 1969 (2007).